At a second glance: cognitive and oculomotor neural activity of refixation planning

Andrey R. Nikolaev[1,2]*, Benedikt V. Ehinger[3], Radha Nila Meghanathan[4], Cees van Leeuwen[2,5]

[1] Department of Psychology, Lund University, Lund, Sweden
[2] Brain & Cognition Research Unit, KU Leuven - University of Leuven, Leuven, Belgium
[3] Stuttgart Center for Simulation Science, University of Stuttgart, Germany
[4] Department of Experimental Psychology, Otto-von-Guericke University Magdeburg, Germany
[5] Center for Cognitive Science, Technical University, Kaiserslautern, Germany

* Corresponding author

Abstract

Evidence has been accumulating for the close relationship between, on the one hand, the neural mechanisms of eye movement control and, on the other, cognitive functions such as perception, attention, and memory. In natural viewing behavior, eye movements drive and coordinate the neural activity of these functions. This, however, makes it a methodologically challenging task to separate neural activity serving oculomotor and cognitive functions during free viewing. Extensive free viewing is characterized by three distinct fixation types: ordinary fixations to locations visited once, precursor fixations to locations that are revisited later, and refixations that are revisits of precursor locations. We simultaneously recorded EEG and eye movement in a free-viewing contour search task and analyzed fixation-related EEG activity in these fixation categories. We applied a regression-based deconvolution approach, which allowed us to account for the overlapping EEG responses due to the saccade sequence, as well as for the contribution of oculomotor variables. We found that the EEG amplitude for precursor fixations differs from that for ordinary fixations and refixations 200-400 ms after the fixation onset, most noticeably over the occipital areas. Follow-up analyses showed that the effect increases if we remove adjustments according to saccade size and order in the fixation sequence (fixation rank), which are distinct for precursor fixations. This implies that brain processes underlying precursor fixations have distinct oculomotor and cognitive components. As our data suggest, the cognitive role of precursor fixations is to demarcate locations strategically important for planning information acquisition in the current task. This observation is supported by the particular oculomotor characteristics of precursor fixations, such as saccade size and fixation rank. Overall, our findings emphasize the active coordinating role of eye movements in cognitive neural mechanisms.

Introduction

About 20 years ago, John Findlay and Ian Gilchrist advanced the groundbreaking concept of active vision, emphasizing the crucial role of eye movement in visual perception and cognition (Findlay and Gilchrist, 2003). Since then, research has emphasized the involvement of brain regions related to eye movements in cognitive functions such as attention and memory. Specific neurons in the lateral intraparietal area and the frontal eye field have spatial receptive fields and saccade-related maps, allowing them to encode attentional selection and send this as feedback to the early visual areas and the subcortical structures that generate saccades (Gottlieb, 2012). Integrated visual and oculomotor signals select targets and, at the same time, trigger the saccades needed to fixate them. This demonstrates the close relationship between the neural circuits controlling eye movements and spatial attention (Awh et al., 2006). The hippocampus builds up a memory, mapping out the spatial and temporal relations between elements on display (Eichenbaum, 2017), guiding eye movements to encode and retrieve pieces of information on a fixation-by-fixation basis (Voss et al., 2017). Eye movements do not simply supply memory with visual information, but also organize its spatial and temporal relationships into sustained representations (Foulsham and Kingstone, 2013; Johansson et al., 2012; Wynn et al., 2019). Thus, eye movements serve as a mechanism for binding visuospatial elements into coherent memory representations (Ryan et al., 2020).

In sum, structurally and functionally interwoven cognitive and oculomotor networks generate eye movements that drive and coordinate cognitive functions (Ryan et al., 2020). As a consequence, eye-movement offsets reflect the exact timing of ongoing cognitive processes. This property has, for instance, been exploited in neurocognitive research for time-series analysis of brain signals (Kragel and Voss, 2022).

The contribution of the oculomotor system to cognitive functions is of particular importance in light of the upcoming transition from laboratory to naturalistic paradigms in psychological research, which is intended to provide the necessary ecological validity to it (Shamay-Tsoory and Mendelsohn, 2019). Consequently, experimental paradigms with unrestricted eye movement behavior are growing in popularity in, among others, studies of reading (Dimigen et al., 2011), memory encoding (Nikolaev et al., 2011), visual search (Kamienkowski et al., 2018; Körner et al., 2014), perception of natural scenes (Coco et al., 2020; Devillez et al., 2015), aesthetic evaluation of art (Fudali-Czyz et al., 2018), and decision making in value judgment (Tyson-Carr et al., 2020).

The brain's reliance on eye movements to support unfolding cognition in space and time brings up a methodological challenge: to what extent can neural signals related to oculomotor behavior be separated out from those related to cognitive functions of interest (Touryan et al., 2017). Causal interventions into eye-movement control are typically only possible for highly artificial experimental conditions (e.g., no free-selection, single eye movements) or highly unnatural stimuli (e.g., Ehinger et al., 2018). We sidestep this issue here and focus on correlative analyses, while non-linearly adjusting for the most dominant oculomotor behaviors. We demonstrate the potential of this technique, applying state-of-the-art statistical approaches to EEG recorded simultaneously with eye movement in free viewing behavior.

EEG is long-known to be heavily affected by eye movements (Evans, 1953). These effects have typically been considered as artifacts, and considerable efforts have been made to develop

methods of removing them (e.g., Lins et al., 1993). Currently, oculomotor (non-neural) artifacts arising from blinks, eyeball rotations, and eye muscle contractions are not a major problem for EEG research anymore, due to the high efficiency of independent component analysis (ICA) for their correction (Jung et al., 2000). Specialized ICA-based approaches can remove oculomotor artifacts from EEG recordings even in free viewing conditions (Dimigen, 2020; Plöchl et al., 2012). The greatest remaining problem of EEG research in natural viewing behavior is overlapping EEG activity evoked by sequential saccades, which may be confused with the cognitive effects of interest. Moreover, low-level eye movement characteristics, such as saccade size, may systematically affect EEG (Dimigen et al., 2011; Nikolaev et al., 2016). To disentangle cognitive from oculomotor neural activity, methods are needed to statistically account for effects of multiple eye movement characteristics on the EEG signal. The current study makes use of deconvolution modeling. Deconvolution modeling enables us to estimate unknown isolated neural responses from the measured EEG and the latencies of experimental and eye movement events (Dimigen and Ehinger, 2021; Ehinger and Dimigen, 2019). Using model comparisons of the various eye movement characteristics, we estimate the relative contribution of oculomotor and cognitive activity to the unadjusted EEG.

We apply this approach to neural activity accompanying three typical categories of fixations in natural viewing behavior. Natural viewing is characterized by frequent returns of the gaze to locations that were visited several seconds ago (Yarbus, 1967). Such refixations constitute up to 35% of eye movements (Beck et al., 2006; Mannan et al., 1997; Zelinsky et al., 2011), suggesting that they represent a common mode of viewing behavior and play an important role in visual perception. Correspondingly, eye movements in free viewing can be divided into three categories: ordinary fixations, precursor fixations, which are the initial fixations of locations to where the eyes will return later, and refixations. In this study, we aim to isolate the neural activity associated with the oculomotor and cognitive components of these three fixation categories, considering them as common and representative of any free viewing behavior.

The cognitive functions of interest stem from studies of refixations in natural viewing behavior. Refixations have been ascribed a range of roles, such as recovering information that was missed or has become lost during scanning (Gilchrist and Harvey, 2000), updating representation of a previously visited location (Tatler et al., 2005); rehearsal of a fading memory representation (Meghanathan et al., 2019; Zander et al., 2011); or compensating for a premature shift of attention away from the fixation (Gilchrist et al., 2001; Peterson et al., 2001). In all these cases, refixations are aimed at restoration of deficiencies arising in information processing and storage.

We propose three explorative hypotheses related to possible differences in the acquisition of visual information at the three fixation categories. First, precursor fixation locations may qualify for a later return if the information acquisition was not, or could not be completed despite the best effort. These locations may contain strategic information or an excess of important detail, and may therefore give rise to a plan to return later. In this case, we should observe larger information acquisition at precursor fixations than at both ordinary fixations and refixations. But information acquisition at refixations and ordinary fixations should be similar because of their equal (un)importance for the exploration plan. Alternatively, information acquisition during initial scanning may have drops due to, e.g., attentional lapses, prompting refixations. Therefore, second, information acquisition in this case should be weaker rather than stronger at precursor fixations than at ordinary fixations, where it should be intermediate. These drops should be compensated by

larger information acquisition at refixations. Thus, information acquisition for all three fixation categories will be different. Third, if refixations are prompted by memory deficits originating after the precursor fixation, for instance, by random forgetting, information acquisition at precursor fixations should not differ from ordinary fixations. But information acquisition at refixations should differ from both precursor and ordinary fixations because lesser amount of information is needed to restore the deficiencies.

To test these hypotheses, we used a previously recorded simultaneous EEG and eye movement dataset of a free-viewing contour integration task. We considered EEG relative to the fixation onset and used deconvolution modeling to obtain model coefficients (betas), which are analogous to fixation-related potentials (FRPs) time-locked to fixation onsets. FRPs reflect perception and initial encoding of visual information at each fixation (Kamienkowski et al., 2018; Kazai and Yagi, 2003; Ries et al., 2016). To study information acquisition at the three fixation categories, we compared the FRP amplitude between them. Our key manipulation involved the evaluation of additive, non-linear effects of a number of eye movement covariates to the deconvolution model, such as XY fixation positions, fixation duration and saccade size and angle. Moreover, the serial position of fixations within a trial of a free viewing task, fixation rank, may affect FRPs (Fischer et al., 2013; Kamienkowski et al., 2018). Since refixations always occur after precursor fixations, we also included fixation rank in the model.

We found that the FRP amplitude, which is corrected for the overlap and fully adjusted for eye movement covariates, differs for precursor fixations from other fixation categories in the interval 200-400 ms after fixation onset. This difference became much larger when saccade size and fixation rank were not included in the model, but did not change when XY positions, fixation duration, and saccade angle were left out of the model. This implies that brain processes associated with fixation categories and saccade size and rank share a common mechanism. Since precursor fixations mostly occur at the beginning of visual exploration and are preceded by large saccades, we propose that the precursor fixation locations are important for the exploration plan. Specifically, we argue that information gathered at precursor fixation locations may contain an excess of important details, and therefore may be of strategic importance and serve as the basis for a plan to return later. This suggests the pivotal role of precursor fixations in planning of acquisition of visual information.

Methods

In the dataset used in this study we previously analyzed EEG in stimulus conditions (Van Humbeeck et al., 2018) and also compared EEG related to refixations and ordinary fixations but not precursor fixations (Nikolaev et al., 2018).

Participants

23 healthy adults (two male) took part in the experiment. Data from two participants were removed: one because of problems during eye movement recording and another because of excessive EEG artifacts. Another three participants were excluded due to interrupted EEG recording, which prevented synchronization of EEG and eye movement data using the EYE-EEG toolbox. The mean age of the remaining 18 participants was 21.7 (range = 18-33) years. All participants gave written informed consent. The study was approved by the Ethics Committee of the Faculty of Psychology and Educational Sciences of KU Leuven.

Stimuli and procedure

Gabor patches of approximately 0.3-0.4° of visual angle were randomly placed with a mean distance of 0.7° between them in large displays of 30 x 30° at a viewing distance of 55 cm. In half of the trials, seven patches formed a contour because their orientation was aligned +/- 25° with the neighboring patches (contour-present trials). The contour was embedded at a random location of the display. In the other half of the trials, the orientation of all patches was random (contour-absent trials).

Participants initiated a trial by pressing the space bar on the computer keyboard. At the beginning of a trial a fixation cross was presented for a random duration between 0.5 and 1 s. Next, a display was presented for 8 s. Contour-present or contour-absent displays were presented in random order. Participants searched for a contour and indicated its presence or absence within the following 5 s response interval by pressing "p" or "q" keys of the computer keyboard. A feedback screen indicated whether the response was correct. 120 contour-present and 120 contour-absent trials were presented. The trials were organized in 6 blocks of 40 trials with two-minute breaks between blocks. A short practice session preceded the experiment.

Eye movement recording

The display size necessitates the use of eye movements to search for a contour. Eye movements were recorded with a desktop version of the EyeLink 1000 eye tracking system (SR Research Ltd., Ontario, Canada). The sampling frequency was 250 Hz. A chinrest stabilized participant's head. A 9-point calibration was performed before each block and whenever it was needed during the block, e.g., if participants occasionally moved their head away from the chinrest. The mean number of calibrations per experiment across participants was 17.7 (range 8-32, SD=7.9). A maximum of 2° error margin between calibration and validation was allowed. The space bar press at the beginning of the trial triggered a drift correction, which allowed tracking errors to be kept within 2°.

EEG recording

EEG was recorded at a sampling rate of 250 Hz using a 256-channel Geodesic Sensor Net (EGI, a Philips company, Eugene, OR, USA). The net included electrodes for recording the vertical and horizontal electrooculogram. The recording reference was Cz. The EEG was filtered online with an analog high-pass filter of 0.1 Hz and a 100-Hz low-pass filter. TTL pulses were sent through a parallel port from the stimulus presentation computer to the eye tracking and EEG systems. The synchronization of EEG and eye movement recordings was performed offline using the EYE-EEG extension (Dimigen et al., 2011) for EEGLAB (Delorme and Makeig, 2004).

Selection of refixations, precursor fixations and ordinary fixations

We considered only contour-absent trials with correct responses, because in these trials, visual search invariably lasted for the full 8 s, whereas discovery of a contour at an unidentified moment would end the search for the remaining interval.

Fixations and saccades were detected in the gaze data using the velocity-based algorithm for saccade detection (Engbert and Mergenthaler, 2006) of the EYE-EEG extension. In each trial, we identified refixations within a sequence of fixations (Fig. 1A). A refixation was defined as a fixation within a radius of 2° of visual angle from a previous fixation. A 2° criterion has repeatedly been used in refixation studies (Anderson et al., 2013; Gilchrist and Harvey, 2000; Solman et al., 2011). It

assures that fixation and a refixation overlap on the fovea. We did not consider as refixations any subsequent fixations prior to leaving the 2° range. If a refixation occurred within 2° from two or more close (<2°) precursor fixations, we scored it as a refixation only once. When two or more sequential refixations occurred, we took only the first one. After applying these criteria, on average, 15.8% (SD = 3.1, range 10.6-22) of eye movements per participant were counted as refixations. We excluded fixations immediately preceding a refixation because these contain preparatory EEG activity specific for refixations (Nikolaev et al., 2018).

To identify precursor fixations, we selected all fixations that later receive refixations. Their number was slightly less than the number of refixations because several refixations could originate from the same precursor fixation. Precursor fixations and refixations were distributed unequally in time, skewing towards the left and right edge of a trial, respectively (Fig. 1B). Precursor fixations and refixations were separated by, on average, 9 (SD = 1.2, range 7-10.9) intervening fixations.

To select ordinary fixations, we excluded precursor fixations and refixations (also the ones discarded during the selection) from all the fixations in a trial. The number of ordinary fixations was much larger than that of precursor fixations and refixations. Therefore, we randomly selected a number of ordinary fixations, equal to the mean number of precursor fixations and refixations. The excluded ordinary fixations as well as the fixations discarded during selection of other fixation categories (see above) were assigned to the condition of 'other' fixations, as we will specify in the Deconvolution section below. Alternatively, we could have modelled each category separately, by estimating their own FRPs. But because some categories do not have many trials, their individual FRP estimates would be too noisy. Thus, by combining categories, we traded-off increased bias for decreased variance.

EEG cleaning

The EEG data processing consisted of two main parts: cleaning the EEG data, and modelling the overlapping effects of sequential eye movements and the influence of eye movement covariates on the EEG. Since modelling the overlapping effects involves time regression it cannot be done on EEG segments. Therefore the cleaning was performed on the continuous EEG.

We analyzed 148 of the 256 electrodes: 108 electrodes close to the cheeks and neck were removed because they often had poor contact due to the long hair of our mostly female participants, and showed strong muscle artifacts. For cleaning we used functions from the EEGLAB toolbox for MATLAB. First, we applied the *pop_cleanline* function, which removes power line noise from EEG using multi-tapering, and a Thompson F-statistic. Then we applied *clean_artifacts*, which removes flat-line channels, low-frequency drifts, noisy channels, and short-time bursts. To remove transient or large-amplitude artifacts this function uses artifact subspace reconstruction (ASR). It is an automatic, subspace-based method, which compares the structure of the artifactual EEG activity to that of known artifact-free reference data (Kothe and Jung, 2016). The efficiency of ASR for artifact removal crucially depends on the ASR parameter that defines the tradeoff between removing non-brain signals and retaining brain activities. We set the ASR parameter to 20, which was found to be optimal in a dedicated study (Chang et al., 2020).

We removed ocular artifacts in free viewing behavior using the OPTICAT function (Dimigen, 2020). This function performs independent component analysis (ICA) by training ICA on prepared EEG data, which allows to better isolate influences of oculomotor artifacts than with typical ICA on

unprepared EEG data. In particular, EEG was high-pass filtered at 2 Hz but was not low-pass filtered, in order to preserve high-frequency components of the myogenic saccadic spike activity. Furthermore, the contribution of the saccadic spike activity was overweighted in the EEG input to ICA by cutting 30 ms segments around saccade onsets (defined by eye tracking) and re-appending them to the EEG. After ICA training on these filtered data, the obtained ICA weights were transferred to the unfiltered version of the same data. Then the function computed the ratio between the IC mean variance during saccade and fixation intervals and marked ICs as saccade-related if the ratio was higher than 1.1 (Plöchl et al., 2012). The saccade-related ICs were removed. The ICs related to the remaining artifacts were removed with the automatic classifier (*pop_iclabel*). This removed components with parameters muscle 0.4-1, eye 0.9-1, heart 0.05-1, line noise 0.4-1, channel noise 0.4-1, other 0.4-1). The EEG was then recreated without these components. Finally, EEG was filtered with a low cut-off of 0.1 Hz (-6 dB at 0.05 Hz) and with a high cut-off of 30 Hz (-6 dB at 30.05 Hz) using the *pop_eegfiltnew* function with default settings. EEG was re-referenced to average reference. The removed channels (mean = 10.5, SD = 7.3 per participant) were interpolated with spherical spline interpolation.

Deconvolution

Due to the non-uniform distribution of fixation durations, effects of sequential eye movements in natural viewing behavior on EEG are systematic and may confound effects of experimental conditions. Moreover, low-level oculomotor characteristics, such as fixation duration, X and Y positions of a fixation on the screen, the size and direction of saccades, *per se* may affect fixation-related EEG (Dimigen and Ehinger, 2021; Dimigen et al., 2011; Nikolaev et al., 2016). Furthermore, the fixation rank, i.e., the position in the order of fixations within a trial, may influence fixation-related potentials during a trial with multiple eye movements (Fischer et al., 2013; Kamienkowski et al., 2018). In addition, the EEG response evoked by the onset of the stimulus screen may distort the following fixation-related potentials (Dimigen et al., 2011; Gert et al., 2021). To eliminate these effects, we used the deconvolution approach implemented in the Unfold toolbox for MATLAB (Ehinger and Dimigen, 2019). The toolbox performs a regression-based EEG analysis that includes mass univariate modeling, linear deconvolution modeling, and generalized additive modeling. As a result, it computes the partial effects (i.e., the beta coefficients or "regression ERPs, rERPs") for predictors of interest, adjusted for all other covariates. The analysis with the Unfold toolbox consists of four major steps, which are described in detail in (Ehinger and Dimigen, 2019) and are illustrated with respect to different data types in (Dimigen and Ehinger, 2021).

First, we specified the regression model and generated the design matrix. According to the Wilkinson notation, the model formula was defined as follows:

Fixation: y ~ 1 + fixationCategory + spl(rank,5) + spl(duration,5) + spl(fix_avgpos_x,5) + spl(fix_avgpos_y,5) + spl(sac_amplitude,5) + circspl(sac_angle,5,-180,180)'
Stimulus: y ~1

Levels of *fixationCategory*: Other (reference level), Ordinary, Precursor, Refixation

The formula indicates that we considered multiple effects of the fixation event and the stimulus onset event. Specifically, for fixations, we considered as covariates the fixation onset (y ~ 1, i.e., the intercept), the fixation conditions of main interest as a categorical predictor ('fixationCategory'), and fixation rank, fixation duration, X and Y fixation positions, the size (amplitude) and the angle of the preceding saccade. The fixation category predictor included four levels: 'other' fixations (see

above), ordinary fixations, precursor fixations, and refixations. We used treatment coding with 'other' as the reference level. Since we assumed that the fixation rank, duration, X and Y fixation positions as well as the saccade size and angle have nonlinear effects on EEG, we modeled them with a basis set of five spline predictors (saccade angle – with circular splines). Spline knots were placed on the participant-specific percentiles of the covariates (i.e., on the 3 ($N_{splines}$-2 = 5-2) quantiles). For stimulus events, we included in the model only their onsets (y ~ 1), i.e., the intercept that indicated the shape of the overall waveform of the potential evoked by the image.

Second, the design matrix was time-expanded in a time window between −200 and +500 ms around fixation and stimulus onset events. The time expansion generated a new design matrix for the continuous EEG, based on the classical mass univariate linear regression design matrix (number of events x 29 predictors) and the onset of all modelled events. Each stimulus and eye-movement event is modelled by a set of time-lagged impulse response functions, one for each time lag – weighted by their respective mass-univariate design-matrix value (for a detailed explanation see Ehinger & Dimigen (2019)). Because this new design matrix is defined for all time points of the continuous EEG, we estimate a single linear model instead of estimating many linear models. This allows us to simultaneously estimate all stimulus and fixation betas. The variable temporal distance between sequential events allows us to separate their overlapping effects. The time-expanded design matrix spanned the duration of the entire EEG recording. It had 5075 (29 predictors x 250 Hz x 0.7 s) columns and several thousand rows, the number of which varied across participants.

Third, we excluded artifactual time-periods by setting entire rows of the time-expanded design matrix to zero. Doing so, we removed from the model the inter-trial intervals, the breaks between blocks, the contour-present trials, the trials with incorrect responses, the trials without refixations, and bad eye-tracking intervals. Then, the deconvolution model was fitted for each of the 148 electrodes using the iterative Least Squares Minimal Residual algorithm (Fong and Saunders, 2011) for sparse design matrices.

Fourth, we reconstructed averaged EEG waveforms ("regression-based fixation-related potentials", rEFPs) from the beta coefficients of the model for three fixation conditions. rEFPs were considered from 200 ms before and 500 ms after the fixation onset. To adjust for the covariate effects, we calculated marginal effects of the mean. That is, for each covariate (e.g., saccade size) we determined the participant-wise average covariate value (e.g., 7.3°) and evaluated the effect-rEFP at this value. This value was then added to all other predictors, effectively adjusting all resulting rEFPs to the same covariate-values. These rEFPs are equivalent to participant-level averages in a traditional ERP analysis. For the main analysis, rEFPs were baseline-corrected at -200 -100 ms before the fixation onset, an interval that does not knowingly include saccade execution.

Statistical analysis

Deconvolution was done for each participant separately. To perform the statistical analysis on the group level we estimated the FRP amplitude in unbiased time windows based on the grand average and *a priori* regions of interest (ROIs). Since the number of *a priori* tests is typically small, the issue of multiple comparisons for them is minor, which increases the statistical power of the tests. Moreover, they are more likely to detect narrowly distributed effects that occur across a small number of time points and electrodes (Groppe et al., 2011). We selected eight ROIs over the left and right hemisphere, namely, frontal, central, parietal and occipital brain regions, which were defined around landmark electrodes of the International 10-20 System of Electrode Placement: F3,

F4, C3, C4, P3, P4, O1, O2 (the inset in Fig. 2A). For each ROI, we averaged amplitudes over one central and six surrounding electrodes. This approach involved 56 (=7 x 8) electrodes, symmetrically and systematically distributed over the head. Such an approach is generally suggested for high-density electrode montages (Dien and Santuzzi, 2005). Based on visual inspection of the grand-averaged FRPs we selected two time windows. The first, lambda time window included +/-2 sampling points from the lambda peak at 80 ms after the fixation onset: 72-88 ms. The second, late time window was chosen to include the most pronounced FRP negativity over the occipital regions 200-400 ms after the fixation onset.

The FRP amplitudes were compared between fixation categories with a repeated-measures ANOVA. The Huynh-Feldt correction for p-values associated with two or more degrees of freedom was applied in case of sphericity violation. Fisher's LSD (least significant difference) test was used for post-hoc analyses. The statistical analyses were performed with STATISTICA 10 (StatSoft Inc., Tulsa, OK, USA) and R version 4.0.2 (2020).

For the FRP amplitude in the lambda time window, we considered only the occipital ROIs (OL and OR) because here the lambda activity is maximal (Kazai and Yagi, 2003; Thickbroom et al., 1991; Yagi, 1979). Therefore, the ANOVA had two factors: Fixation category (Precursor Fixation, Refixation, Ordinary Fixation) and Hemisphere (left, right). For the late time window, we considered all 8 ROIs, and therefore the ANOVA had three factors: Fixation category (Precursor Fixation, Refixation, Ordinary Fixation), ROI (frontal, central, parietal, occipital), and Hemisphere (left, right).

Results

Eye movement results

There were on average 203 (range 130-270, SD=42.5) precursor fixations and 216 (range 138-286, SD=47.5) refixations per participant. The number of ordinary fixations was artificially made equal to the average number of these fixations, as mentioned earlier.

For fixation duration, a repeated-measures ANOVA with the factor of Fixation category (precursor fixations, refixations, ordinary fixations) showed no significant difference ($F(2, 34) = 0.9$, $p = .4$) (the inset in Fig. 1B). Although the shapes of the fixation duration distributions were quite similar for all fixation categories, the peak of the precursor fixation duration distribution was slightly higher than in the other two categories (Fig. 1B), suggesting a difference in spread of the distribution. This could affect FRP results because the distribution peaked at about 250 ms, indicating that the onset for the maximum number of subsequent saccades, was in the time window of the FRP analysis (200-400 ms after the fixation onset). To test a possible difference in distributions we applied a shift function that estimates how and by how much one distribution has to be shifted to match the other one (Rousselet et al., 2017). The shift function calculates the decile differences between two distributions as a function of the deciles of the first distribution. For each decile difference, it computes 95% confidence intervals with bootstrap estimation of the standard error of the deciles. If the confidence interval does not comprise zero, the difference is considered significant with an alpha of .05. We computed two shift functions: for the difference between the distributions of precursor and ordinary fixation duration (Fig. 1C) and the difference between the distributions of precursor and refixation fixation duration (Fig. 1D). In both cases, the confidence intervals

comprised zero, indicating that the differences between the shapes of the distributions were insignificant.

The effect of Fixation category on saccade size was highly significant ($F(2, 34) = 22$, $p < .001$, $\varepsilon = 1$); saccades were largest for precursor fixations and smallest for refixations (all post-hoc $p < .004$) (Fig. 1F). A circular ANOVA (the R package 'Circular', v0.4-93; (Lund and Agostinelli, 2017)) on data pooled across participants also showed a significant difference in saccade angles between fixation categories ($F(2, 11313) = 115$, $p < .001$) (Fig. 1G). For the post-hoc test of saccade angles we used the Watson's two-sample test of homogeneity. Saccade angles for refixations differed from those for precursor and ordinary fixations (both $p < .01$), whereas saccade angles did not differ between precursor and ordinary fixations ($p > .1$). Fixation positions were compared separately for X and Y positions. No significant effects of fixation categories on fixation positions were found (Fig. 1H).

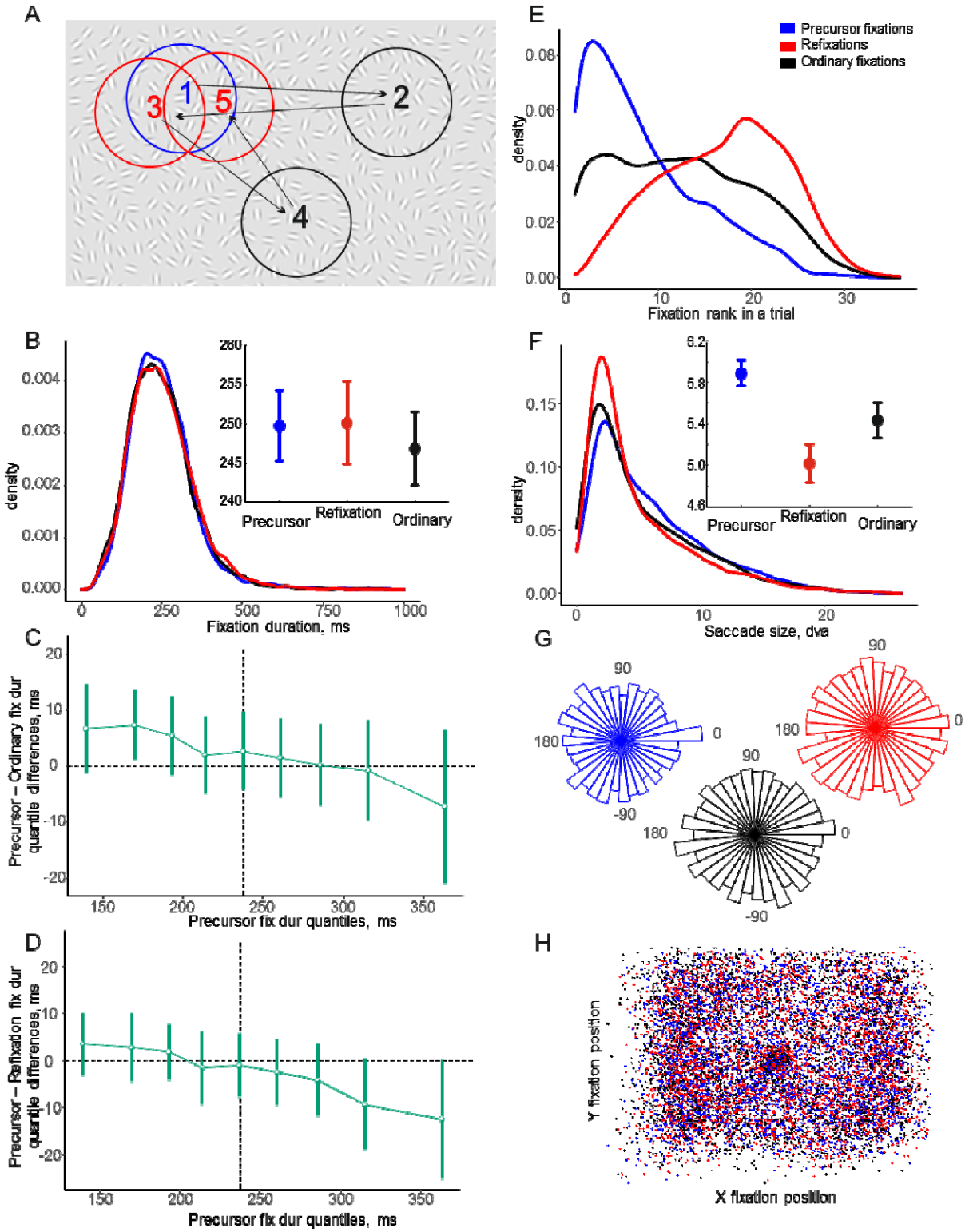

Fig. 1. A: Fixation categories. Circles represent areas within a radius of 2° of visual angle around the fixation point. Numbers indicate an order (rank) of subsequent fixations. Fixation 1 is a precursor fixation; fixations 2 and 4 are ordinary fixations; fixations 3 and 5 are refixations. B: Probability density estimation of fixation duration. The inset shows a mean-error plot, where the error bars indicate the standard errors of the means across 18 participants. C: Shift function for the distributions of precursor and ordinary fixation duration. Error bars indicate the 95% bootstrap confidence interval. D: Shift function for the distributions of precursor and refixation fixation duration. E: Probability

density estimation of fixation rank within an 8-s trial. F: Probability density estimation of saccade size. G: Distribution of saccade angles. H: Distribution of fixation positions on the screen, pooled across 18 participants.

EEG results

The effect of fixation categories on FRP

Fig. 2A illustrates the effects of deconvolution and addition of covariates to the model on FRPs in the three fixation categories. To evaluate effects of the deconvolution correction we built two additional models – one included mass linear univariate modeling and another included deconvolution without addition of covariates. The left panel in Fig. 2A shows the FRPs without deconvolution and addition of covariates, which were obtained with mass univariate modelling (*uf_glmfit_nodc*). The central panel shows the FRPs with deconvolution but without addition of covariates. The right panel shows the fully adjusted FRPs, i.e., with deconvolution and addition of covariates, which illustrate the main result.

Topographical maps for 148 electrodes showed a positive peak, equally large for all three fixation categories. The peak was narrowly localized over the occipital areas 100 ms after the fixation onset – the lambda wave (Fig. 2B). At 300 ms after fixation onset, a prominent negativity was spread over the parieto-occipital areas and was mirrored over the frontal areas. The area of negativity over the parieto-occipital areas was larger for precursor fixations than for refixations and ordinary fixations.

In the lambda time window, there was a prominent effect of Fixation category on the FRPs without deconvolution and addition of covariates, as well as on the FRPs with deconvolution but without addition of covariates (Table 1). The lambda peak amplitude was higher for refixations than for ordinary fixations and larger for ordinary fixations than for precursor fixations (all post-hoc $p < .001$). The effect of Hemisphere was also significant with higher FRPs over the right than over the left hemisphere (all post-hoc $p < .001$), with no interaction. Since the fixation categories differed in saccade size (Fig. 1F), the well-known effect of saccade size on lambda amplitude (Dimigen et al., 2011; Yagi, 1979) was expected. Interestingly, the direction of the differences in the unadjusted lambda amplitude between the three fixation categories corresponds to differences in the peaks of the saccade size density (refixations > ordinary fixations > precursor fixations) rather than differences in the mean saccade sizes (precursor fixations > ordinary fixations > refixations) (Fig. 1F), supporting a nonlinear influence of saccade size on the lambda wave (Dimigen and Ehinger, 2021; Nikolaev et al., 2016; Ries et al., 2016). However, after deconvolution and addition of covariates, no effects of fixation category and hemisphere on the lambda amplitude were found.

In the late time window, the results were qualitatively the same for all three models: the FRP amplitude for precursor fixations was significantly different from other fixation conditions, with a maximal difference at approximately 250 ms after the fixation onset. There was also an interaction between Fixation category and ROI, indicating that the difference mostly occurred over the frontal and occipital ROIs. However, the prominence of all effects was much smaller for the FRPs with deconvolution and addition of covariates than in the two non-adjusted models (Table 1).

Since the fully adjusted FRPs after deconvolution and addition of covariates is the main model of our interest, and the results in the other two models were qualitatively similar to it, we will further report and illustrate the results of this model only. The post-hoc test revealed a lower FRP amplitude for the precursor fixations than the refixations and ordinary fixations (all $p < .03$) (Fig. 2C). We found significant effects of ROI and Hemisphere and an interaction between them (all $p <$

.03). More importantly, we found an interaction between Fixation category and ROI ($F(6, 102) = 3.5$, $p = .03$, $\varepsilon = .44$). The post-hoc tests revealed a lower FRP amplitude for the precursor fixations than for the refixations and ordinary fixations over the occipital ROIs (all $p < .005$) and a larger FRP amplitude over the frontal ROIs (all $p < .05$). There was no difference between the refixations and ordinary fixations (Fig. 2D).

Thus, deconvolution reduces the overlapping effect about 250 ms after the fixation onset, compared to the mass univariate modelling, but does not affect the difference at the lambda peak. Adding covariates to the model removes the effect of saccade size on the lambda peak and further reduces the overlap. Most importantly, the FRPs for precursor fixations still differ from other fixation categories after deconvolution and addition of covariates, indicating that factors other than overlap and eye movement covariates contribute to this effect.

Table 1. The ANOVA results for three FRP models: 1) without deconvolution and addition of covariates (No deconv, no covar); 2) with deconvolution but without addition of covariates (Deconv, no covar); 3) with deconvolution and addition of covariates (Deconv, covar). For the lambda time window only the main fixation category effect is reported because only occipital areas were considered. For the late time window, the main fixation category effect and the interaction between Fixation category and ROI are reported.

Time window relative to the fixation onset	Effects	No deconv, no covar	Deconv, no covar	Deconv, covar
Lambda (72-88 ms)	Fixation category, $df = 2, 34$	$F = 9.0$, $p < .001$, $\varepsilon = 1$	$F = 8.3$, $p = .001$, $\varepsilon = 1$	$F = 1.3$, $p = .29$, $\varepsilon = 1$
Late (200-400 ms)	Fixation category, $df = 2, 34$	$F = 9.8$, $p < .001$, $\varepsilon = 1$	$F = 8.9$, $p < .001$, $\varepsilon = 1$	$F = 3.5$, $p = .04$, $\varepsilon = 1$
	Fix. category x ROI, $df = 6, 102$	$F = 12.9$, $p < .001$, $\varepsilon = .42$	$F = 10.7$, $p < .001$, $\varepsilon = .46$	$F = 3.5$, $p = .03$, $\varepsilon = .44$

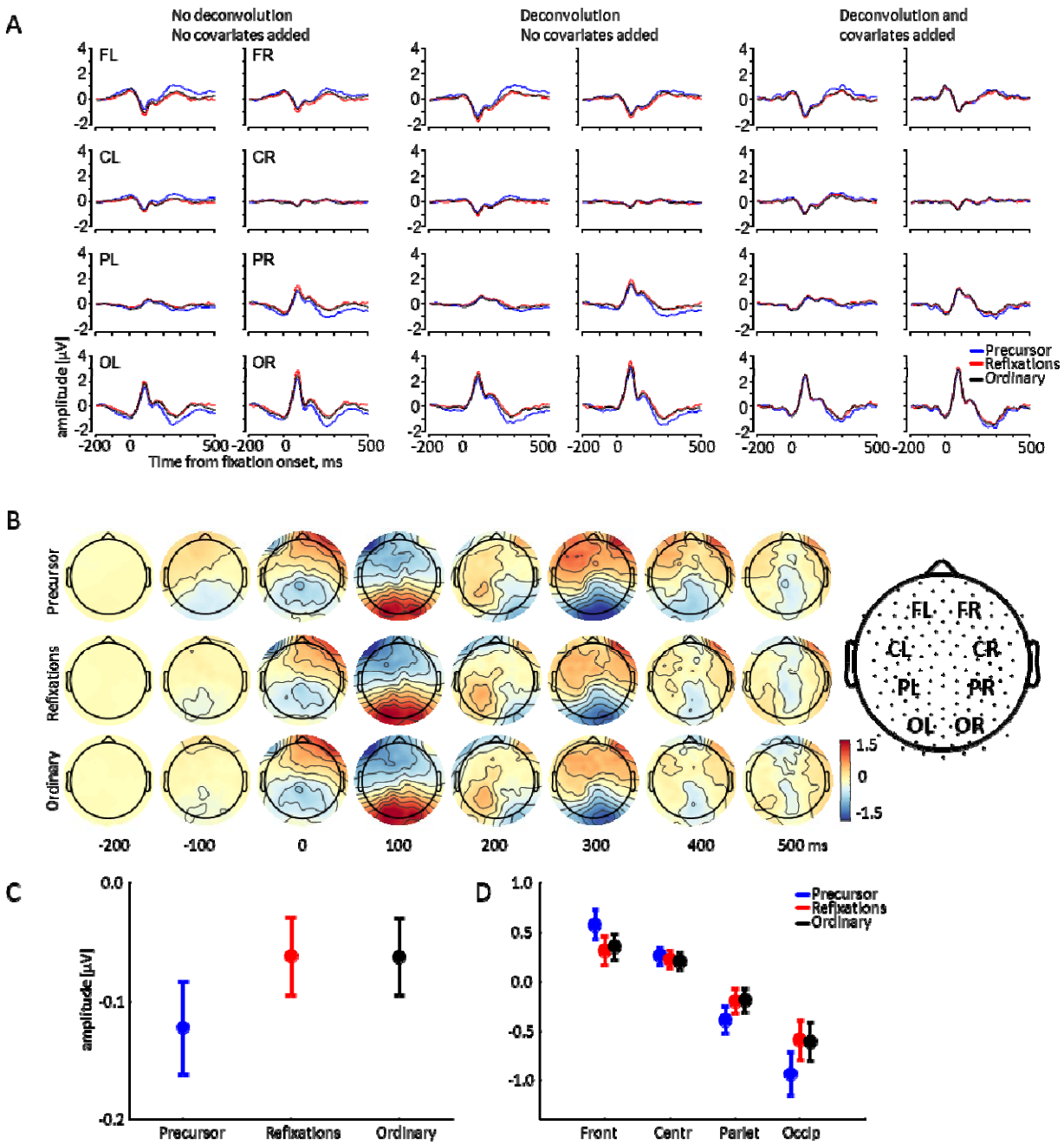

Fig. 2. The fixation-related potentials (regression betas) time-locked to the fixation onset for three fixation categories. The potentials are grand-averaged (N=18) and baseline-corrected at -200 -100 ms before the fixation onset. A: The fixation-related potentials for 8 ROIs for three models (see the text). B: The topographical maps over 148 electrodes. The inset at the bottom indicates locations of 8 regions of interest (ROIs): left and right frontal (FL, FR), central (CL, CR), parietal (PL, PR), occipital (OL, OR). C: The mean amplitude in the interval 200-400 ms after fixation onset, indicating the main effect of the fixation category. D: The mean amplitude in the interval 200-400 ms after fixation onset, indicating the interaction between the fixation category and ROI. Error bars indicate standard errors of the means across 18 participants.

Control analysis with a baseline interval from 0 to 20 ms

Since the choice of the baseline interval for analysis of FRPs in free viewing is not a trivial task (Nikolaev et al., 2016), we corroborated the reliability of the observed difference between fixation

categories in a control analysis with a baseline interval from 0 to 20 ms after the fixation onset. It is assumed that this interval is free from the influence of saccade preparation and execution, while the perception-related EEG activity has not yet begun (Rama and Baccino, 2010).

We ran the same ANOVAs as before. The results were generally consistent with those using the baseline at -200 -100 ms before the fixation onset for fully adjusted FRPs (Fig. 3A). Specifically, we found neither significant effects nor interactions in the lambda window. For the late time window, we found an effect of Fixation category ($F(2, 34) = 8.2$, $p = .001$, $\varepsilon = 1$). The post-hoc test revealed a lower FRP amplitude for the precursor fixations than for the refixations and ordinary fixations (all $p < .03$) (Fig. 3B). We found an interaction between Fixation category and ROI ($F(6, 102) = 5.3$, $p = .004$, $\varepsilon = .46$). The post-hoc test revealed a lower FRP amplitude for the precursor fixations than for the refixations and ordinary fixations over the occipital ROIs (all $p < .006$) and a larger FRP amplitude over the frontal ROIs (all $p < .05$) (Fig. 3C). The difference between precursor and ordinary fixations over the parietal ROIs was also significant (p = .008). But we did not find significant effects nor an interaction for ROI and Hemisphere. Thus, the choice of the baseline interval does not affect the peculiarities of precursor fixations.

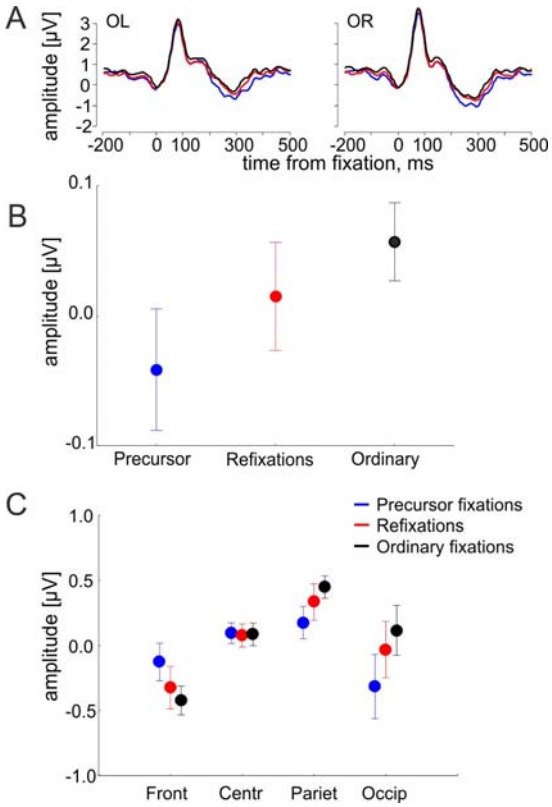

Fig. 3. The FRP results of the control analysis with the different baseline interval: 0-20 ms from the fixation onset. A: The fully adjusted FRPs for the left and right occipital (OL, OR) ROIs, where the effect in the interval 200-400 ms was most prominent. B: The mean amplitude in the interval 200-400 ms after fixation onset, indicating the main effect of the fixation category. C: The mean amplitude in the interval 200-400 ms after fixation onset, indicating the interaction between the fixation category and ROI. Error bars indicate standard errors of the means across 18 participants.

Contribution of oculomotor covariates to the fixation categories effect

To investigate the relative contribution of cognitive and oculomotor activity to the fixation category FRP effect, we ran a series of deconvolution models from which each or all oculomotor covariates

were removed. We reasoned that if the removal of any covariate would result in a significant change of the fixation category effect in the same time window and with the same topography, this would indicate linked mechanisms for the cognitive effect observed in the fully adjusted model and the oculomotor process related to that covariate.

We expected that the fixation rank, saccade size and angle may be the covariates that are most informative about the possible mechanism about the fixation category effect, because they differed between the fixation categories (Fig. 1E-G). Moreover, fixation duration may also be involved, as the average fixation duration in our task was about 250 ms (Fig. 1B), and therefore the late time window (200-400 ms after fixation onset) included the onset latency of a large number of subsequent saccades which evoked EEG responses that overlapped with the response to the current saccade.

We removed each predictor one at a time from the formula of the fully adjusted model (fixation positions X and Y were removed simultaneously), and we also ran the fully confounded model without predictors (Table 2). The intercept of the stimulus onset was added to the formulas, as in the main analysis. We assessed the fixation category effect across models by F-value of the main effect of fixation categories in the same ANOVA design as in the main analysis. We quantified the effect size in each model by the difference between the mean FRP amplitude in the late time window for precursor and ordinary fixations over the right occipital ROI, where the effect was maximal.

Table 2. The names of the models and the formulas used to model fixation-related events. The covariates in bold were in the formula; the covariates in regular font *were not* in the formula and are only shown to emphasize the difference of each formula.

The name of the model	Formula used in the modeling fixations
Fully adjusted (the main analysis)	**y~1+cat(code)+spl(rank,5)+spl(duration,5)+spl(fix_avgpos_x,5)+spl(fix_avgpos_y,5)+spl(sac_amplitude,5)+circspl(sac_angle,5,-180,180)**
No XY positions	**y~1+cat(code)+spl(rank,5)+spl(duration,5)+**spl(fix_avgpos_x,5)+spl(fix_avgpos_y,5)+**spl(sac_amplitude,5)+circspl(sac_angle,5,-180,180)**
No fixation duration	**y~1+cat(code)+spl(rank,5)+**spl(duration,5)+**spl(fix_avgpos_x,5)+spl(fix_avgpos_y,5)+spl(sac_amplitude,5)+circspl(sac_angle,5,-180,180)**
No saccade angle	**y~1+cat(code)+spl(rank,5)+spl(duration,5)+spl(fix_avgpos_x,5)+spl(fix_avgpos_y,5)+spl(sac_amplitude,5)+**circspl(sac_angle,5,-180,180)
No saccade size	**y~1+cat(code)+spl(rank,5)+spl(duration,5)+spl(fix_avgpos_x,5)+spl(fix_avgpos_y,5)+**spl(sac_amplitude,5)+**circspl(sac_angle,5,-180,180)**
No rank	**y~1+cat(code)+**spl(rank,5)+**spl(duration,5)+spl(fix_avgpos_x,5)+spl(fix_avgpos_y,5)+spl(sac_amplitude,5)+circspl(sac_angle,5,-180,180)**
Fully confounded	**y~1+cat(code)**+spl(rank,5)+spl(duration,5)+spl(fix_avgpos_x,5)+spl(fix_avgpos_y,5)+spl(sac_amplitude,5)+circspl(sac_angle,5,-180,180)

Fig. 4 shows the results of the seven models described in Table 2. Fig. 4A demonstrates the FRP waveforms of the three fixation categories over the right occipital ROI. The effect of fixation categories was significant in all models, except the model without XY positions, and was largest for the fully confounded model, where the FRP for precursor fixations deviated maximally from the other fixation categories (Fig. 4B). A repeated-measures ANOVA on the FRP amplitude difference between precursor and ordinary fixations over the right occipital area for the different models indicated a significant increase in effect from the fully adjusted to the fully confounded model ($F(6, 102) = 13.3$, $p < .001$, $\varepsilon = .39$) (Fig. 4C). The post-hoc test showed that this increase was due to the difference between the fully adjusted, no XY, no fixation duration, and no saccade angle models on the one hand *versus* no saccade size, no rank, and fully confounded models on the other hand. Fully adjusted, no XY, no fixation duration, and no saccade angle models did not differ from each other (all $p > .15$). No saccade size and no rank models also did not differ from each other ($p = .7$), but did differ from the fully confounded model (both $p < .002$).

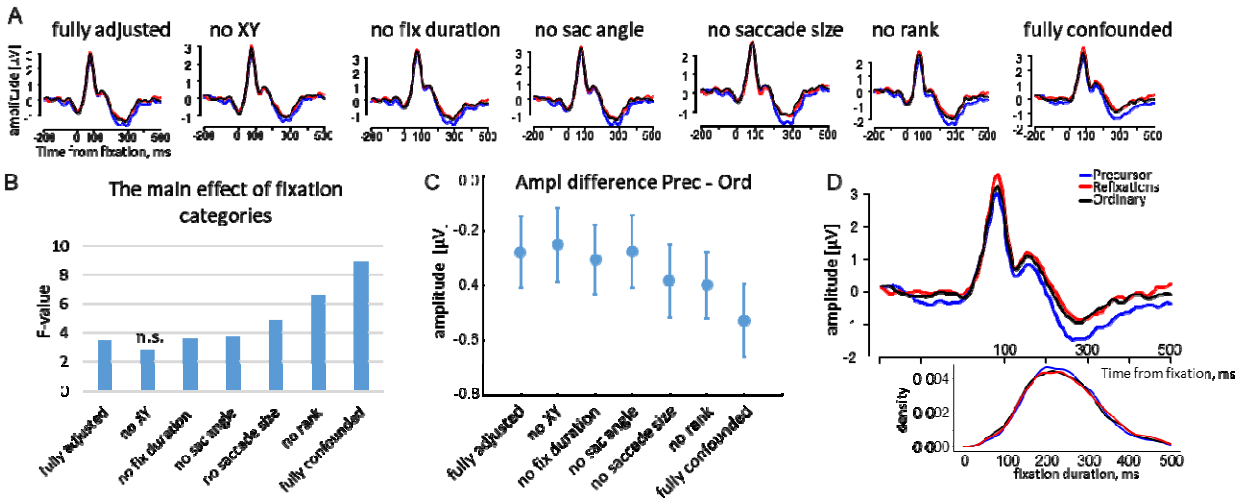

Fig. 4. Results of seven models with and without some or all continuous predictors. A: The fixation-related potentials for the right occipital ROI, where the fixation category effect was maximal, for seven models designated in Table 2. B: F-values of the main effect of fixation categories for the seven models. C: The amplitude difference (precursor minus ordinary fixations) over the right occipital ROI for the seven models. Error bars indicate standard errors of the means across 18 participants. D: The close-up for FRP over the right occipital ROI for the fully confounded model with the probability density of fixation duration, indicating the distribution of onsets of the subsequent saccade.

Discussion

We aimed to disentangle cognitive and oculomotor neural activity related to three typical categories of fixations in naturalistic viewing behavior. We considered EEG signals relative to the onsets of precursor fixations, refixations, and ordinary fixations. We applied regression-based deconvolution modeling to adjust the fixation-related EEG for overlapping effects and effects of multiple eye movement covariates. The fully adjusted FRP amplitude differed for precursor fixations from the amplitude for ordinary fixations and refixations 200-400 ms after the fixation onset, most noticeably over the occipital areas. The finding that the effect remains after all oculomotor variables were removed from the data shows that these neural signals have a distinctive cognitive component. To assess the contribution of cognitive and oculomotor factors to this fixation category effect, we performed a series of follow up analyses, which showed that if saccade size and fixation rank are not adjusted, the fixation category effect with the same latency and topography increases, while this does not apply to other eye movement characteristics.

The effect of fixation categories on FRP is about the same in the fully adjusted model and when XY positions, fixation duration and saccade angle are not adjusted. This indicates a negligible contribution of these eye movement characteristics to the fixation category effect. However, the fixation category effect becomes significantly larger in the fully confounded model or when fixation rank and saccade size are not adjusted. The greatest effect in the fully confounded model results from the joint removal of fixation rank and saccade size from the model, which are interdependent in the time course of a free-viewing trial. Particularly, it is well known that saccades are largest at the beginning of a free-viewing trial, whereas saccade size decreases later, reflecting the transition from exploratory to scrutinizing viewing strategies (Fischer et al., 2013; Pannasch et al., 2008;

Unema et al., 2005). Respectively, precursor fixations, which are characterized by the earliest fixation rank compared to other fixation categories, are preceded by the largest saccades. This feature of precursor fixations correlates with their FRP amplitude and thus represents an oculomotor neural component of the fixation category effect.

The cognitive neural component of the fixation category effect could be understood in relation to the late time window of its occurrence in the fully adjusted model. This time window corresponds to the onset latency of subsequent saccades, but the effect did not change when we excluded the fixation duration, which is indicative of the latency, from the model. Moreover, the contribution of subsequent saccades to the effect is unlikely, because deconvolution accounted for their overlapping FRP activity. The late time window is close to the window (250-400 ms after the fixation onset) where the dependence of FRP amplitude on fixation rank was previously reported in a free-viewing visual search task. There, the effect was explained by integrative cognitive processes associated with search progression (Kamienkowski et al., 2018). Furthermore, lambda activity, which is known to reflect perception at each fixation (Dimigen et al., 2009; Kazai and Yagi, 1999; Ossandón et al., 2010; Thickbroom et al., 1991), was not affected by fixation categories in the fully adjusted model. All these findings suggest a cognitive rather than perceptual origin of the processes supporting precursor fixations. In our contour integration task, these processes are elicited after large exploratory saccades, which may serve to demarcate the visual stimulus (Gabor's field) into locations that should be remembered for future revisits. In particular, according to the first hypothesis proposed in the introduction, the precursor fixation locations contain an excess of strategic information and therefore may give rise to a plan to return later. At the beginning of visual exploration, these strategic locations may be spotted at the periphery and reached by large saccades. To build the exploration plan, information acquisition may be increased during the precursor fixations following large saccades, as evidenced by the larger amplitude of the late FRP component for precursor fixations than for ordinary fixations and refixations. Then, during refixations, only some additional details are acquired, because most of the information is already captured at precursor fixations when the plan was made. The amount of information in these details appeared to be the same as in ordinary fixation locations, as indicated by the equal FRP amplitude for refixations and ordinary fixations. The ordinary fixations probably occur at "uninteresting" locations that are considered uninformative about the target contour.

On the other hand, the possibility remains that the effects of saccade size and fixation rank have not been fully corrected and spill over into FRPs even in the fully adjusted model. While our flexible spline basis sets can theoretically approximate a large class of smooth non-linear relationships, overfitting on condition-dependent noise or simply unlucky sampling could still bias our results. This notwithstanding, the Unfold toolbox appears to be highly efficient in correcting the effects of eye movement covariates. This can be concluded from the disappearance of the saccade size effect in the lambda time window when it was added to the model as a covariate, so the saccade size effect in the fully adjusted model should be corrected in the late time window as well. Therefore, we conclude the probability of the spillover is negligible and that the neural mechanism underlying the fixation category effect on FRPs has cognitive and oculomotor components.

Conclusions

A growing understanding of the intimate link between the cognitive and oculomotor brain systems is supported by research showing that eye movements do not simply supply our vision with information or passively reflect the outputs of visual processing, but are themselves an inextricable part of the attention and memory brain systems (Awh et al., 2006; Gottlieb, 2012; Voss et al., 2017). Our study extends this understanding by showing the relative contributions of cognitive and oculomotor components to the difference between the three basic categories of fixations in free viewing behavior. Using deconvolution allowed us to separate fixation-related neural responses. Precursor fixations to locations that are subsequently refixated have distinct neural correlates compared to refixations and ordinary fixations. While the neural mechanisms of refixations have been investigated earlier (Kragel et al., 2021; Meghanathan et al., 2020; Nikolaev et al., 2018), to the best of our knowledge, the neural correlates of the precursor fixations have not been studied before. Their peculiarity may arise from the combined contribution of cognitive factors responsible for making a strategic plan of visual exploration, and oculomotor factors that determine the size of saccades depending on their serial position (rank) in a trial. These findings emphasize the intertwined character of cognitive processing and oculomotor behavior.

Acknowledgments

ARN and RNM were supported by an Odysseus grant (G.0003.12) from the Flemish Organization for Science (FWO) to Cees van Leeuwen. ARN was also supported by a grant from the Marcus and Amelia Wallenberg Foundation (MAW2015.0043) to Mikael Johansson. BE was funded by Deutsche Forschungsgemeinschaft (DFG, German Research Foundation) under Germany´s Excellence Strategy – EXC 2075 – 390740016. We thank Nathalie Van Humbeeck and Johan Wagemans for permission to use the jointly collected data in this study.

References

Anderson, N.C., Bischof, W.F., Laidlaw, K.E., Risko, E.F., Kingstone, A., 2013. Recurrence quantification analysis of eye movements. Behavior research methods 45, 842-856.

Awh, E., Armstrong, K.M., Moore, T., 2006. Visual and oculomotor selection: links, causes and implications for spatial attention. Trends in cognitive sciences 10, 124-130.

Beck, M.R., Peterson, M.S., Vomela, M., 2006. Memory for where, but not what, is used during visual search. Journal of Experimental Psychology: Human Perception and Performance 32, 235-250.

Chang, C.Y., Hsu, S.H., Pion-Tonachini, L., Jung, T.P., 2020. Evaluation of Artifact Subspace Reconstruction for Automatic Artifact Components Removal in Multi-Channel EEG Recordings. IEEE Transactions on Biomedical Engineering 67, 1114-1121.

Coco, M.I., Nuthmann, A., Dimigen, O., 2020. Fixation-related Brain Potentials during Semantic Integration of Object-Scene Information. Journal of Cognitive Neuroscience 32, 571-589.

Delorme, A., Makeig, S., 2004. EEGLAB: an open source toolbox for analysis of single-trial EEG dynamics including independent component analysis. Journal of Neuroscience Methods 134, 9-21.

Devillez, H., Guyader, N., Guerin-Dugue, A., 2015. An eye fixation-related potentials analysis of the P300 potential for fixations onto a target object when exploring natural scenes. Journal of vision 15, 20.

Dien, J., Santuzzi, A.M., 2005. Application of repeated measures ANOVA to high density ERP datasets: A review and tutorial. In: Handy, T.C. (Ed.), Event-related potentials: A methods handbook MIT Press, Cambridge, MA, pp. 57– 82.

Dimigen, O., 2020. Optimizing the ICA-based removal of ocular EEG artifacts from free viewing experiments. Neuroimage 207, 116117.

Dimigen, O., Ehinger, B.V., 2021. Regression-based analysis of combined EEG and eye-tracking data: Theory and applications. Journal of vision 21, 3.

Dimigen, O., Sommer, W., Hohlfeld, A., Jacobs, A.M., Kliegl, R., 2011. Coregistration of eye movements and EEG in natural reading: analyses and review. Journal of Experimental Psychology: General 140, 552-572.

Dimigen, O., Valsecchi, M., Sommer, W., Kliegl, R., 2009. Human microsaccade-related visual brain responses. Journal of Neuroscience 29, 12321-12331.

Ehinger, B.V., Dimigen, O., 2019. Unfold: an integrated toolbox for overlap correction, non-linear modeling, and regression-based EEG analysis. PeerJ 7, e7838.

Ehinger, B.V., Kaufhold, L., Konig, P., 2018. Probing the temporal dynamics of the exploration-exploitation dilemma of eye movements. Journal of vision 18, 6.

Eichenbaum, H., 2017. On the Integration of Space, Time, and Memory. Neuron 95, 1007-1018.

Engbert, R., Mergenthaler, K., 2006. Microsaccades are triggered by low retinal image slip. Proceedings of the National Academy of Sciences of the United States of America 103, 7192-7197.

Evans, C.C., 1953. Spontaneous excitation of the visual cortex and association areas; lambda waves. Electroencephalography and Clinical Neurophysiology 5, 69-74.

Findlay, J.M., Gilchrist, I.D., 2003. Active vision. Oxford University Press, New York.

Fischer, T., Graupner, S.T., Velichkovsky, B.M., Pannasch, S., 2013. Attentional dynamics during free picture viewing: evidence from oculomotor behavior and electrocortical activity. Frontiers in systems neuroscience 7, 17.

Fong, D.C.L., Saunders, M., 2011. Lsmr: An Iterative Algorithm for Sparse Least-Squares Problems. Siam Journal on Scientific Computing 33, 2950-2971.

Foulsham, T., Kingstone, A., 2013. Fixation-dependent memory for natural scenes: an experimental test of scanpath theory. Journal of Experimental Psychology: General 142, 41-56.

Fudali-Czyz, A., Francuz, P., Augustynowicz, P., 2018. The Effect of Art Expertise on Eye Fixation-Related Potentials During Aesthetic Judgment Task in Focal and Ambient Modes. Front Psychol 9, 1972.

Gert, A.L., Ehinger, B.V., Timm, S., Kietzmann, T.C., König, P., 2021. Wild lab: A naturalistic free viewing experiment reveals previously unknown EEG signatures of face processing. bioRxiv, 1-28.

Gilchrist, I.D., Harvey, M., 2000. Refixation frequency and memory mechanisms in visual search. Current Biology 10, 1209-1212.

Gilchrist, I.D., North, A., Hood, B., 2001. Is visual search really like foraging? Perception 30, 1459-1464.

Gottlieb, J., 2012. Attention, learning, and the value of information. Neuron 76, 281-295.

Groppe, D.M., Urbach, T.P., Kutas, M., 2011. Mass univariate analysis of event-related brain potentials/fields I: a critical tutorial review. Psychophysiology 48, 1711-1725.

Johansson, R., Holsanova, J., Dewhurst, R., Holmqvist, K., 2012. Eye movements during scene recollection have a functional role, but they are not reinstatements of those produced during encoding. Journal of Experimental Psychology: Human Perception and Performance 38, 1289-1314.

Jung, T.P., Makeig, S., Humphries, C., Lee, T.W., McKeown, M.J., Iragui, V., Sejnowski, T.J., 2000. Removing electroencephalographic artifacts by blind source separation. Psychophysiology 37, 163-178.

Kamienkowski, J.E., Varatharajah, A., Sigman, M., Ison, M.J., 2018. Parsing a mental program: Fixation-related brain signatures of unitary operations and routines in natural visual search. Neuroimage 183, 73-86.

Kazai, K., Yagi, A., 1999. Integrated effect of stimulation at fixation points on EFRP (eye-fixation related brain potentials). International Journal of Psychophysiology 32, 193-203.

Kazai, K., Yagi, A., 2003. Comparison between the lambda response of eye-fixation-related potentials and the P100 component of pattern-reversal visual evoked potentials. Cognitive, affective & behavioral neuroscience 3, 46-56.

Körner, C., Braunstein, V., Stangl, M., Schlogl, A., Neuper, C., Ischebeck, A., 2014. Sequential effects in continued visual search: using fixation-related potentials to compare distractor processing before and after target detection. Psychophysiology 51, 385-395.

Kothe, C.A.E., Jung, T.-P., 2016. Artifact removal techniques with signal reconstruction. In: App, U.P. (Ed.), USA.

Kragel, J.E., Schuele, S., VanHaerents, S., Rosenow, J.M., Voss, J.L., 2021. Rapid coordination of effective learning by the human hippocampus. Sci Adv 7.

Kragel, J.E., Voss, J.L., 2022. Looking for the neural basis of memory. Trends in cognitive sciences 26, 53-65.

Lins, O.G., Picton, T.W., Berg, P., Scherg, M., 1993. Ocular artifacts in EEG and event-related potentials. I: Scalp topography. Brain Topography 6, 51-63.

Lund, U., Agostinelli, C., 2017. Package 'circular'. Repository CRAN, 1-142.

Mannan, S.K., Ruddock, K.H., Wooding, D.S., 1997. Fixation sequences made during visual examination of briefly presented 2D images. Spatial Vision 11, 157-178.

Meghanathan, R.N., Nikolaev, A.R., van Leeuwen, C., 2019. Refixation patterns reveal memory-encoding strategies in free viewing. Atten Percept Psychophys 81, 2499-2516.

Meghanathan, R.N., van Leeuwen, C., Giannini, M., Nikolaev, A.R., 2020. Neural correlates of task-related refixation behavior. Vision Research 175, 90-101.

Nikolaev, A.R., Meghanathan, R.N., van Leeuwen, C., 2016. Combining EEG and eye movement recording in free viewing: pitfalls and possibilities. Brain and Cognition 107, 55-83.

Nikolaev, A.R., Meghanathan, R.N., van Leeuwen, C., 2018. Refixation control in free viewing: a specialized mechanism divulged by eye-movement related brain activity. Journal of Neurophysiology 120, 2311-2324.

Nikolaev, A.R., Nakatani, C., Plomp, G., Jurica, P., van Leeuwen, C., 2011. Eye fixation-related potentials in free viewing identify encoding failures in change detection. Neuroimage 56, 1598-1607.

Ossandón, J.P., Helo, A.V., Montefusco-Siegmund, R., Maldonado, P.E., 2010. Superposition model predicts EEG occipital activity during free viewing of natural scenes. Journal of Neuroscience 30, 4787-4795.

Pannasch, S., Helmert, J.R., Roth, K., Herbold, A.K., Walter, H., 2008. Visual fixation durations and saccade amplitudes: shifting relationship in a variety of conditions. Journal of Eye Movement Research 2, 1-19.

Peterson, M.S., Kramer, A.F., Wang, R.X.F., Irwin, D.E., McCarley, J.S., 2001. Visual search has memory. Psychological science 12, 287-292.

Plöchl, M., Ossandón, J.P., König, P., 2012. Combining EEG and eye tracking: identification, characterization, and correction of eye movement artifacts in electroencephalographic data. Frontiers in human neuroscience 6, 278.

Rama, P., Baccino, T., 2010. Eye fixation-related potentials (EFRPs) during object identification. Visual Neuroscience 27, 187-192.

Ries, A.J., Touryan, J., Ahrens, B., Connolly, P., 2016. The Impact of Task Demands on Fixation-Related Brain Potentials during Guided Search. PLoS One 11, e0157260.

Rousselet, G.A., Pernet, C.R., Wilcox, R.R., 2017. Beyond differences in means: robust graphical methods to compare two groups in neuroscience. European Journal of Neuroscience 46, 1738-1748.

Ryan, J.D., Shen, K., Liu, Z.X., 2020. The intersection between the oculomotor and hippocampal memory systems: empirical developments and clinical implications. Annals of the New York Academy of Sciences 1464, 115-141.

Shamay-Tsoory, S.G., Mendelsohn, A., 2019. Real-Life Neuroscience: An Ecological Approach to Brain and Behavior Research. Perspect Psychol Sci 14, 841-859.

Solman, G.J., Allan Cheyne, J., Smilek, D., 2011. Memory load affects visual search processes without influencing search efficiency. Vision Research 51, 1185-1191.

Tatler, B.W., Gilchrist, I.D., Land, M.F., 2005. Visual memory for objects in natural scenes: from fixations to object files. Quarterly Journal of Experimental Psychology. A, Human Experimental Psychology 58, 931-960.

Thickbroom, G.W., Knezevic, W., Carroll, W.M., Mastaglia, F.L., 1991. Saccade onset and offset lambda waves: relation to pattern movement visually evoked potentials. Brain Research 551, 150-156.

Touryan, J., Lawhern, V.J., Connolly, P.M., Bigdely-Shamlo, N., Ries, A.J., 2017. Isolating Discriminant Neural Activity in the Presence of Eye Movements and Concurrent Task Demands. Frontiers in human neuroscience 11, 357.

Tyson-Carr, J., Soto, V., Kokmotou, K., Roberts, H., Fallon, N., Byrne, A., Giesbrecht, T., Stancak, A., 2020. Neural underpinnings of value-guided choice during auction tasks: An eye-fixation related potentials study. Neuroimage 204, 116213.

Unema, P.J.A., Pannasch, S., Joos, M., Velichkovsky, B.M., 2005. Time course of information processing during scene perception: the relationship between saccade amplitude and fixation duration. Visual Cognition 12, 473-494.

Van Humbeeck, N., Meghanathan, R.N., Wagemans, J., van Leeuwen, C., Nikolaev, A.R., 2018. Presaccadic EEG activity predicts visual saliency in free-viewing contour integration. Psychophysiology 55, e13267.

Voss, J.L., Bridge, D.J., Cohen, N.J., Walker, J.A., 2017. A Closer Look at the Hippocampus and Memory. Trends in cognitive sciences 21, 577-588.

Wynn, J.S., Shen, K., Ryan, J.D., 2019. Eye Movements Actively Reinstate Spatiotemporal Mnemonic Content. Vision (Basel) 3.

Yagi, A., 1979. Saccade size and lambda complex in man. Physiological Psychology 7, 370-376.

Yarbus, A.L., 1967. Eye movements and vision. Plenum Press, New York.

Zander, T.O., Gaertner, M., Kothe, C., Vilimek, R., 2011. Combining eye gaze input with a brain-computer interface for touchless human-computer interaction. International Journal of Human-Computer Interaction 27, 38-51.

Zelinsky, G.J., Loschky, L.C., Dickinson, C.A., 2011. Do object refixations during scene viewing indicate rehearsal in visual working memory? Memory and Cognition 39, 600-613.